Development 139, 3817-3826 (2012) doi:10.1242/dev.084053

Evidence for karyoplasmic homeostasis during endoreduplication and a ploidy-dependent increase in gene transcription during tomato fruit growth

Matthieu Bourdon[1,2,*], Julien Pirrello[2,*], Catherine Cheniclet[2,6], Olivier Coriton[3], Mickaël Bourge[4], Spencer Brown[5], Adeline Moïse[2], Martine Peypelut[2,6], Valérie Rouyère[1], Jean-Pierre Renaudin[1], Christian Chevalier[2,‡] and Nathalie Frangne[1]

SUMMARY

Endopolyploidy is a widespread process that corresponds to the amplification of the genome in the absence of mitosis. In tomato, very high ploidy levels (up to 256C) are reached during fruit development, concomitant with very large cell sizes. Using cellular approaches (fluorescence and electron microscopy) we provide a structural analysis of endoreduplicated nuclei at the level of chromatin and nucleolar organisation, nuclear shape and relationship with other cellular organelles such as mitochondria. We demonstrate that endopolyploidy in pericarp leads to the formation of polytene chromosomes and markedly affects nuclear structure. Nuclei manifest a complex shape, with numerous deep grooves that are filled with mitochondria, affording a fairly constant ratio between nuclear surface and nuclear volume. We provide the first direct evidence that endopolyploidy plays a role in increased transcription of rRNA and mRNA on a per-nucleus basis. Overall, our results provide quantitative evidence in favour of the karyoplasmic theory and show that endoreduplication is associated with complex cellular organisation during tomato fruit development.

KEY WORDS: Endoreduplication, Nuclear structure, Tomato, Fruit development, Transcription

INTRODUCTION

Variation in cell ploidy levels, termed somatic endopolyploidy, is part of normal development and physiology in many eukaryotic organisms, ranging from insects to mammals and plants (Brodsky and Uryvaeva, 1977). As a widespread phenomenon, endopolyploidy can result from several mechanisms, such as the generation of multinucleate cells originating from acytokinetic mitosis, nuclear fusion, endomitosis or from endoreduplication. The last two mechanisms represent the most frequently encountered modes of polyploidisation in eukaryotes (Lee et al., 2010). During endomitosis, chromosomes double and condense, sister chromatids separate normally, but chromosomes return to the interphase state within a single nucleus, thus doubling the chromosome number. Although present in various phyla, endomitosis is rare in the plant kingdom (D'Amato, 1984). Rather, endoreduplication is the major source of endopolyploidy in higher plants, particularly in angiosperms in which it arises in most species and in many different tissues (Nagl, 1976; D'Amato, 1984). During endoreduplication, endonuclear DNA duplication occurs in the absence of any obvious condensation and decondensation steps, thus producing chromosomes with multivalent (2, 4, 8, 16, etc.) chromatids without any change in chromosome number (Joubès and Chevalier, 2000).

The adaptive value of endoreduplication during plant development is not fully understood, and various functional hypotheses have arisen in the literature. As an inducer of nuclear DNA amplification, endoreduplication has been proposed to provide a means to sustain growth under adverse environmental conditions, such as genotoxic stress (Hase et al., 2006; Adachi et al., 2011), saline stress (Ceccarelli et al., 2006), water deficit (Cookson et al., 2006) and low temperature (Barow, 2006).

The most obvious role for endoreduplication during plant development has been ascribed to the determination of cell size, as positive correlations between endoreduplication and cell size are classically observed in many plant species, organs and cell types (Chevalier et al., 2011). According to the 'karyoplasmic ratio' theory, successive endocycles influence the final size of the cell, which tends to adjust its cytoplasmic volume with respect to the nuclear DNA content (for a review, see Sugimoto-Shirasu and Roberts, 2003).

As far as morphogenesis is concerned, endoreduplication may impact not only the final size of the cell but also its differentiation. In *Arabidopsis*, four rounds of endoreduplication are required during the developmental programme of epidermal hair cells called trichomes in order to produce mature many-branched single cells with an average DNA content of 32C (Hülskamp et al., 1999), and a direct correlation between the ploidy level and the number of branches does occur: mutations that affect the number of endocycles lead to trichomes with supernumerary or reduced numbers of branches (Ishida et al., 2008). As an important determinant of cell identity, endoreduplication was recently demonstrated to be crucial for cell fate acquisition and maintenance, thus contributing to the formation of specialised cell type patterns (Bramsiepe et al., 2010; Roeder et al., 2010). Related

[1]University of Bordeaux, UMR1332 Biologie du Fruit et Pathologie, BP 81, F-33140 Villenave d'Ornon, France. [2]INRA, Unité Mixte de Recherche, 1332 Biologie du Fruit et Pathologie, BP 81, F-33140 Villenave d'Ornon, France. [3]INRA, UMR1349 Institut de Génétique, Environnement et Protection des Plantes (IGEPP), BP 35327, F-35653 Le Rheu, France. [4]CNRS, IFR 87, La Plante et son Environnement, Imagif, F-91198 Gif-sur-Yvette, France. [5]CNRS, Institut des Sciences du Végétal, UPR 2355 and FRC 3115, F-91198 Gif-sur-Yvette, France. [6]CNRS, Bordeaux Imaging Center, UMS 3420, F-33000 Bordeaux, France.

*These authors contributed equally to this work
‡Author for correspondence (chevalie@bordeaux.inra.fr)

Accepted 31 July 2012

to cell specialisation, numerous correlative examples from the animal and plant kingdoms have led to the popular proposal that when associated with highly metabolically active cells, endoreduplication would support an increase in transcriptional and metabolic activities (Lee et al., 2010). However, this proposal has never been clearly demonstrated.

Investigating endoreduplication in tomato (*Solanum lycopersicum* Mill.) is pertinent, not only because elevated levels of endopolyploidy occur in the course of fruit development when compared with other plant organs and species, but also because it does contribute to cell and fruit growth in a developmentally and genetically regulated manner (reviewed by Chevalier et al., 2011). Recently, we developed a fluorescent in situ hybridisation method that allowed us to establish a ploidy map of tomato pericarp at the mature green stage (Bourdon et al., 2011), thereby overcoming the difficulty of determining ploidy at the cellular level in a tissue context. To pave the way towards an understanding of the functional role of endoreduplication during tomato fruit development, we have performed a structural and molecular analysis of endoreduplicated nuclei in fruit pericarp and provide the first direct evidence for a ploidy-dependent increase in gene transcription.

MATERIALS AND METHODS

Plant material and growth conditions

Cherry tomato (*Solanum lycopersicum* Mill. cv Wva106) plants were grown in a greenhouse under a thermoperiod of 25°C/20°C and a photoperiod of 14/10 hours (day/night). Fruits were harvested at the mature green stage [29-32 days post-anthesis (dpa)].

Nuclei sorting

Tomato pericarp nuclei were prepared, sorted by flow cytometry and fixed on microscope slides as described (Bourdon et al., 2011).

Fluorescence techniques

For Chromomycin A3 labelling experiments, three fruits were used to prepare slides containing 500 nuclei of each ploidy level (2C to 128C) sorted directly onto three-well microscope glass slides (Superfrost, CML, France) prepared with a cushion of 20 µl 500 mM sucrose, 22 mM $MgCl_2$, 15 mM sodium citrate, 10 mM MOPS pH 7, 2% formaldehyde and 50 µg/ml Chromomycin A3. Image acquisition was performed promptly after sorting using a Leica DMI6000 microscope with a 20× objective and excitation (Ex) and emission (Em) wavelengths as follow: Ex 450-490 nm, Em long-pass 515 nm.

For 3,3′-dihexyloxacarbocyanine iodide [$DiOC_6(3)$] labelling experiments, equatorial fragments of 30 dpa fruit pericarp were fixed under vacuum infiltration at 20 kPa for 1 hour at 20°C in 4% paraformaldehyde in 0.1 M phosphate buffer pH 7.2. Fixed tissues were left in the fixative solution overnight then washed for 10 minutes in 0.1 M phosphate buffer. A vibrating blade microtome was used to obtain 150 µm sections as described (Bourdon et al., 2011). Staining was performed for 10 minutes in a 1.75 µM $DiOC_6(3)$ solution in 0.1 M phosphate buffer pH 7.2. For Rhodamine-123 labelling experiments (Emaus et al., 1986), handmade equatorial slices were prepared. Staining was performed for 1 minute in 0.5 µM Rhodamine-123, 0.1 M phosphate buffer pH 7.2 supplemented with 0.3 M sorbitol. For both labelling experiments the sections were washed for 1 minute in their respective buffers, and stained for 1 minute with 10 µg/ml DAPI. Sections were then mounted on microscope slides in the same respective buffer and immediately observed by confocal microscopy using the following wavelengths: for $DiOC_6(3)$, Ex 488 nm and Em 505-555; for Rhodamine-123, Ex 496 nm and Em 500-560 nm.

Two anti-RNA polymerase II (RNA pol II) antibodies (S2P and NP) were used for dual immunolabelling of nuclear suspensions supplemented with 5% BSA and 0.3% Triton X-100 (to eliminate plastid fluorescence). Nuclei were washed in 1.5 ml tubes by centrifugation (800 ***g***, 4 minutes) through this buffer supplemented with 0.5 M sucrose, onto a 2 M sucrose cushion. For each of 5000 nuclei classified for ploidy by simultaneous DAPI staining, the immunolabelling intensities of each antibody (S2P and NP; secondary antibodies labelled with Alexa Fluor 633 and Alexa Fluor 488, respectively) and their ratio (S2P/NP) was determined by flow cytometry. Fluorescent images of the nuclei were recorded as *z*-series on a confocal laser-scanning microscope (Leica, Scanhead TCS-SP2 on a DMRXA2) with a 63×/NA1.4 HCX PL APO objective, using the following wavelengths: Ex 488 nm, Em 507-594 nm. For image acquisition of DAPI/transmission pericarp slices, a Nikon DM5000 epifluorescence microscope equipped with a CCD CoolSNAP HQ2 (Photometrics) was used and the fluorescence was recovered with a 450-490 nm band pass filter under Ex 340-380 nm.

DNA and RNA fluorescent in situ hybridisation (FISH)

For FISH experiments, three fruits were used for preparing slides containing up to 2000 nuclei of a given ploidy level (2C to 128C). Nuclei were sorted on slides covered with a 10 µl 500 mM sucrose cushion, allowed to dry at room temperature and stored at –20°C.

DNA FISH was performed as described (Bourdon et al., 2011) using a 45S rDNA ribosomal probe corresponding to a 9 kb *Eco*RI fragment encoding the *Triticum aestivum* 45S rDNA repeat unit (18S-5.8S-26S genes and spacers) (Gerlach and Bedbrook, 1979).

For RNA FISH, antisense and sense (negative control) probes for the 5.8S sequence of the tomato 45S rDNA transcription unit were amplified by PCR using tomato (cv Microtom) genomic DNA and the set of primers described in supplementary material Table S1. Amplicons were purified on an agarose gel using the Wizard PCR Preps DNA Purification System (Promega). Digoxigenin (DIG)-labelled RNA probes were synthesized by in vitro transcription using T7 RNA polymerase and the SP6/T7 DIG RNA Labelling Kit (Roche Diagnostics) according to the manufacturer's instructions. RNA FISH was performed directly after nuclei isolation as described (Jolly et al., 1997). Nuclei were prepared on ice from ~2 mm thick sections of 30 dpa fruit pericarp by gentle chopping in 1 ml CyStain UV ploidy buffer (Partec). The suspension was filtered through a 30 µm nylon mesh directly onto a 400 µl 2 M sucrose cushion in the same buffer and centrifuged at 1200 ***g*** for 10 minutes at 4°C in order to pellet amyloplasts. Then, 150 µl of this suspension were recovered just over the cushion interface and gently homogenised by pipetting. Finally, 10 µl of this homogenate were spread on pasteurised glass microscope slides and allowed to dry for 10-15 minutes. The prepared nuclei were then subjected to fixation, permeabilisation and dehydration steps as described in protocol 3 of Jolly et al. (Jolly et al., 1997). Hybridisation conditions and post-hybridisation washes were as used for DNA FISH on isolated interphase nuclei as described (Bourdon et al., 2011). Signal detection of DIG-labelled probes was carried out with anti-DIG-fluorescein (Roche Diagnostics) for 1 hour in 4× SSC, 0.2% Tween 20 solution according to the manufacturer's instructions. The nuclei were finally mounted and counterstained in Vectashield (Vector Laboratories) containing 1.5 µg/ml DAPI. Three negative controls were performed to confirm the specificity of this protocol: (1) hybridisation with the T7 transcribed 5.8S sense probe described above; (2) a 1 hour treatment with RNase immediately after the nuclei isolation step; (3) hybridisation with a mock treatment (DEPC-treated water instead of the DIG-labelled probe).

Fluorescent images of nuclei were recorded as described above using a confocal laser-scanning microscope and the following wavelengths: for 45S and 5S rDNA FISH (Texas Red), Ex 543 nm and Em 570-675 nm; for 5.8S rRNA FISH (fluorescein), Ex 488 nm and Em 500-550 nm; for DAPI, Ex 405 nm and Em 430-490 nm.

Quantitative (q) PCR

Tomato pericarp fragments were chopped in 3 ml Galbraith's extraction buffer (Galbraith et al., 2011) plus 0.1% Triton X-100 and 30 units RNasin Plus RNase inhibitor (Promega) and nuclei were sorted as described (Bourdon et al., 2011). Total nuclear RNA was extracted from 30,000 sorted nuclei using Trizol reagent (Invitrogen), purified using the RNeasy Mini Kit (Qiagen), and then treated with 0.06 units/µl DNA-free TURBO DNase (Ambion) to remove genomic DNA. The reverse transcription of total nuclear RNA was performed using I-Script (Bio-Rad) in the presence of random primers. The cDNA obtained was diluted 1/10 in distilled water. For real-time PCR, reaction mixes (20 µl) were prepared with 10 µl GoTaq

qPCR Master Mix (Promega), 0.4 µM each primer and 5 µl diluted cDNA. To monitor gene amplification on genomic DNA, 100 sorted nuclei previously boiled for 5 minutes were added to the reaction mix instead of diluted cDNA. PCR amplifications were carried out using a Q-PCR iCycler (Bio-Rad) as: an initial denaturation step of 5 minutes at 95°C, followed by 40 cycles of 15 seconds at 95°C and 25 seconds at 58°C. Data were expressed as relative gene expression normalised to the Ct value obtained for the 32C sample. Primers used in qPCR and RT-PCR experiments are listed in supplementary material Table S2.

RNA pol II immunocytolocalisation

Pericarp slices were fixed for 1 hour in 4% formaldehyde in Tris buffered saline (TBS; 10 mM Tris pH 7.5, 154 mM NaCl) under vacuum infiltration at 20 kPa. Fixed tissues were then washed twice for 5 minutes each in TBS and 150 µm sections were obtained using a vibrating blade microtome. The sections were incubated in blocking solution (5% BSA in TBS) for 30 minutes at 37°C, and washed in TBS for 5 minutes. The polyclonal rabbit anti-RNA pol II S2P (phosphorylated on Ser2; Abcam 5095) or NP (non-phosphorylated; Abcam 817) primary antibodies were diluted 1:200 in TBS containing 0.1% Tween 20 and 5% BSA, and sections were incubated overnight at 4°C. Samples were washed three times for 10 minutes each in TBS and incubated overnight at 4°C with goat anti-rabbit IgG-Alexa 488 (Invitrogen) diluted 1:100 in TBS containing 0.1% Tween 20 and 5% BSA. After three washes in TBS for 5 minutes each, pericarp slices were mounted and counterstained as described above.

Transmission electron microscopy (TEM)

Pericarp fragments were fixed under partial vacuum (20 kPa) in 2.5% glutaraldehyde in 150 mM phosphate buffer pH 7.2 for 4-6 hours at 4°C. After three washes in phosphate buffer (successively 200 mM, 150 mM and 100 mM), the samples were post-fixed in 1% osmium tetroxide in 100 mM phosphate buffer for 3 hours at 4°C, rinsed with phosphate buffer (100 mM then 50 mM) and finally water. An additional fixation step was performed in 1% tannic acid (BDH) in water for 30 minutes at room temperature. Tissues were dehydrated at 4°C through an ethanol series and embedded in Epon according to Carde (Carde, 1987).

Ultrathin sections (50 nm) were stained with 7% uranyl acetate in 50% ethanol and optionally with lead citrate. Digital images were acquired on a CM10 (FEI) transmission electron microscope with an AMT side-port camera (Elexience).

Image analysis

All measurements and counting were with Image-Pro Plus 6.2 software (Media Cybernetics), except for nuclear volumes which were measured with ImageJ software (NIH).

On TEM images, the nuclear radius was calculated as the mean average of Feret min and Feret max, being respectively the width and length of the smallest rectangle enclosing the nucleus. The nuclear perimeter was measured as the length of the nuclear envelope, including that of enclosed invaginations. Counting of mitochondria on TEM images was performed by tagging the mitochondria close to the nucleus, i.e. within ~1 µm of the nuclear envelope (the mean size of mitochondria in this tissue being 1 µm × 0.5 µm).

For counting mitochondria (stained with Rhodamine-123), the *z*-series were treated by blind deconvolution using AutoQuant X software (Roper Scientific). On each *z*-plane the mitochondria located within the DAPI-stained area or within ~1 µm of this area were manually tagged using Image-Pro Plus, the tags being cumulated for the whole *z*-series. This method ensures that mitochondria that are visible on two successive planes due to poor resolution in the *z*-axis (*z*-step of 1 µm) are not counted twice. The nuclear volumes were estimated after segmentation of each plane of the DAPI *z*-series using the Object Counter 3D plug-in of ImageJ.

RESULTS

Endopolyploidisation in tomato fruit generates polytene chromosomes

The consequences of endopolyploidisation for the spatial organisation of chromosomes in tomato fruit cells was investigated by applying our recently described FISH technique (Bourdon et al., 2011) using flow-sorted nuclei at different ploidy levels and a 45S rDNA probe. Whatever the ploidy level, only two hybridisation signals were detected at the 45S rDNA locus, which is located on chromosome 2 in tomato (Jo et al., 2009), and their relative size correlated with the extent of ploidy (Fig. 1A). The use of Chromomycin A3, a DNA-specific dye that preferentially stains GC-rich regions, such as the nucleolar organising regions (NORs) located on chromosome 2 in the tomato genome (Arumuganathan et al., 1994; Chang et al., 2008), confirmed the 45S rDNA hybridisation profile (Fig. 1B).

Both experiments thus showed that chromosome number is unchanged during endopolyploidisation in tomato fruit tissues, demonstrating the occurrence of polytenic chromosomes as expected for endoreduplication.

Endopolyploidy markedly affects nuclear morphology

Taking advantage of the ‘ploidy map’ across the pericarp of mature green tomato (Bourdon et al., 2011), we analysed nuclear morphology in the three most contrasting pericarp areas in terms of ploidy level: the outer epidermis (OE), which displays very low

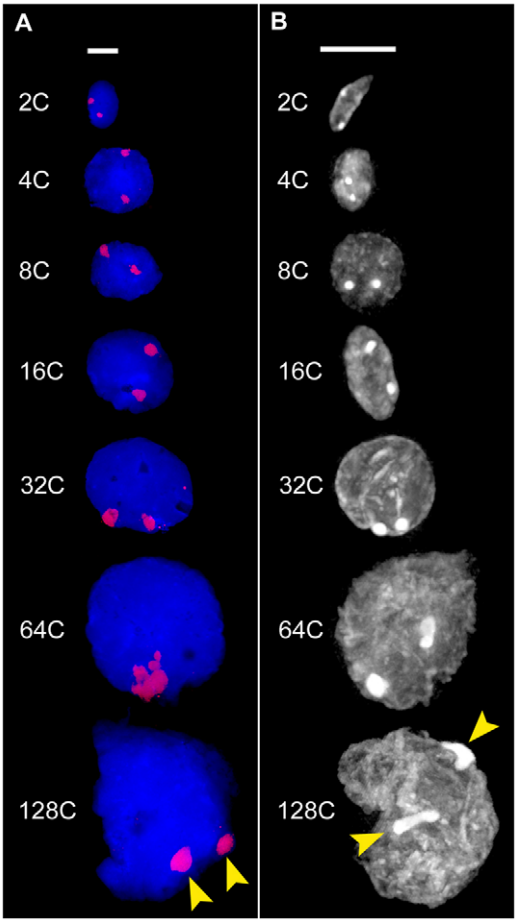

Fig. 1. Endopolyploidisation leads to polytene chromosomes. Tomato nuclei were sorted according to ploidy levels (2C to 128C) by flow cytometry. (**A**) FISH analysis using a wheat 45S rDNA probe and DAPI (blue) to counterstain DNA. (**B**) Chromomycin A3 staining. Arrowheads point to specific DNA hybridisation spots (red, A) and the specifically stained nucleolar organising regions (NORs) (B). Scale bars: 10 µm.

ploidy levels of 2C and 4C; the inner epidermis (IE), which displays mid-ploidy levels ranging from 8C to 32C; and the mid- to inner mesocarp (M), which displays high ploidy levels of 32C to 128C.

Using $DiOC_6(3)$, a lipophilic fluorescent dye that labels intracellular membranes (Terasaki and Reese, 1992), and DAPI, a DNA-specific dye, to stain fruit tissues (Fig. 2A,C,E), small round nuclei were observed in OE (Fig. 2A,B), elongated and slightly grooved nuclei were found in IE (Fig. 2C,D) and large nuclei with numerous invaginations were found in M (Fig. 2E,F). These observations show a clear relationship between the complexity of nuclear shape and the ploidy level. This could be quantified on TEM pictures taking the nuclear area (A), the perimeter (P) corresponding to the length of the nuclear envelope, and the roundness factor (R) according to the formula $R=P^2 \times (4\pi A)^{-1}$ (Fig. 3A). This factor is equal to 1 for a circle and increases for objects diverging from this shape. High values for R were found in pericarp zones of high ploidy levels (M), whereas low values were measured in OE (low ploidy levels) and intermediate values in IE (intermediate ploidy levels). The differences between the three pericarp areas were significant ($P<0.001$, non-parametric Kruskal-Wallis test), which strongly suggests that the extent of the grooves increases according to ploidy.

The development of grooves in polyploid nuclei may impact the exchange ability between the nucleus and cytoplasm. Postulating that nuclear exchange sites (mainly nuclear pore complexes) display the same density all over the nuclear envelope whatever the ploidy level, we hypothesized that the nuclear exchange ability might be represented by a simple ratio between nuclear envelope area and nuclear volume, assuming that the higher this ratio, the higher the nuclear exchange ability. As we performed this analysis on 2D TEM acquisitions, the nuclear envelope area/nuclear volume ratio was estimated as the nuclear P/A ratio and plotted against the mean nuclear radius (r) obtained by averaging the minimum and maximum diameter of each nucleus (Fig. 3B). For a circle, the P/A ratio decreased with r according to an inverse function (y=2/r), thus indicating a lower exchange ability with increasing size. For all measured nuclei, the P/A ratio was higher than for a circle of the same radius. Higher values for P/A may originate from an ellipsoid nuclear shape (especially nuclei from IE) or from an invaginated nuclear shape (especially within M), or from a combination of both. Most nuclei displayed a P/A ratio between 1.6 and 0.6, which corresponds to P/A ratios for circles of 1.3 and 3.3 μm radius, respectively. Even for the biggest nuclei from M (radius >20 μm), the P/A ratio was not lower than that of a 3.3 μm radius circle, indicating that the nuclei could maintain their exchange ability during endopolyploidisation.

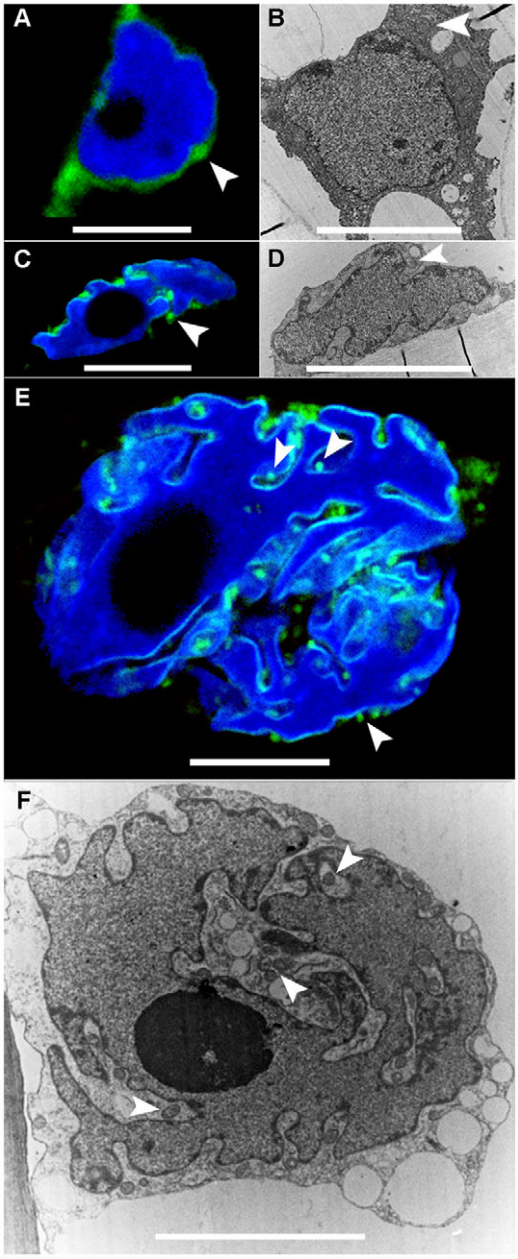

Fig. 2. Complex shape of nuclei associated with ploidy level. (**A-F**) Nuclei in the tomato fruit outer epidermis (OE) (A,B), the inner epidermis (IE) (C,D) and the mesocarp (M) (E,F) were observed by confocal microscopy (A,C,E) and TEM (B,D,F). $DiOC_6(3)$ was used to stain the nuclear envelope (green) and DAPI to counterstain DNA (blue). $DiOC_6(3)$ also reveals endoplasmic reticulum and mitochondria (arrowheads). Scale bars: 5 μm in A,B; 10 μm in C-F.

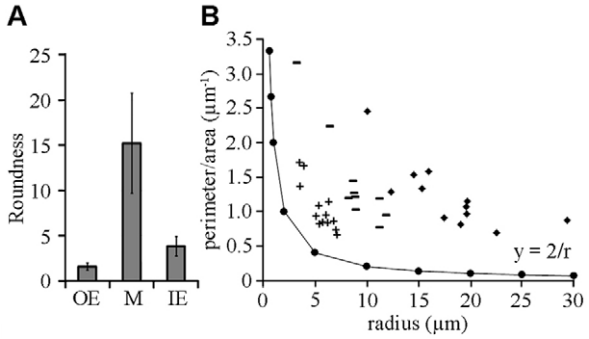

Fig. 3. Maintenance of nuclear-cytoplasm exchange ability during endopolyploidisation. (**A**) Analysis of nuclear shape from TEM images according to position across the tomato fruit pericarp (OE, M and IE) using Image-Pro Plus. Shape is expressed as the roundness parameter (R) (see text). A total of 35 nuclei were analysed for the three zones. The significance of the different R distributions in the three pericarp areas was confirmed by a Mann-Whitney test (α=2.5%). Error bars indicate s.d. (n=13, 12 and 10 for OE, M and IE, respectively. (**B**) Exchange ability of pericarp nuclei according to their size. The exchange ability was estimated as the nuclear perimeter/area (P/A) ratio measured on TEM images of sections of nuclei in OE (crosses), IE (hyphens) and M (diamonds). Nuclear size is expressed as the mean radius (see text). For comparison, the curve (black dots) shows the values of this parameter for circles.

Polyploid nuclei are surrounded by mitochondria

Numerous mitochondria were observed in the close vicinity of polyploid nuclei after $DiOC_6(3)$ staining or in TEM images (Fig. 2E,F). The use of Rhodamine-123, a fluorescent cationic dye used to label mitochondria in living cells (Emaus et al., 1986), confirmed these observations within M (Fig. 4C) and to a lesser extent within IE (Fig. 4B). Only a few mitochondria were seen close to the nuclei within OE (Fig. 4A). Moreover, many mitochondria co-localised with nuclear grooves (Fig. 4C). We then determined the number of mitochondria in proximity to nuclei within the three pericarp areas defined according to the ploidy map (Bourdon et al., 2011). From the *z*-series of confocal images, the mean number of mitochondria surrounding a nucleus (within 1 µm of the nuclear envelope) was ~14.5 in OE, 294 in M and 62 in IE (Fig. 4D). A similar relationship was obtained by counting mitochondria close to the nuclear envelope on TEM images (Fig. 4E), although these values were lower, being derived from single-plane sections of nuclei. Therefore, the number of mitochondria associated with the nuclei increased according to ploidy.

When the above data were expressed as the ratio of mitochondria per nuclear volume or area (Fig. 4F,G), no significant differences appeared between the different pericarp areas ($P>0.08$, Kruskal-Wallis test). Thus, the number of mitochondria relative to nuclear volume or unit area apparently remains constant whatever the ploidy level.

Endoreduplication leads to increased transcription

The developmental process of cell growth requires sustained protein synthesis and thus sustained ribosome biogenesis (Rudra and Warner, 2004). Ribosomal RNAs are transcribed and assembled into ribosomal subunits at the nucleolus (Hernandez-Verdun, 2006). To assess the transcriptional activity associated with the nucleolus, we performed an RNA FISH experiment using 5.8S rRNA as a probe (Fig. 5), which intimately hybridised to the nucleolus (Fig. 5A). The increase in the hybridisation signal area positively correlated with the nuclear area (Fig. 5B), which itself is correlated to ploidy level (Bourdon et al., 2011), thus indicating enhanced transcription for 5.8S rRNA in endoreduplicated nuclei.

To visualise transcriptional activity inside endoreduplicated nuclei from fruit pericarp, in situ immunocytolocalisation experiments were performed to detect the active form of RNA polymerase II (RNA pol II) using an antibody against the phosphorylated heptapeptide YSPTSPS repeat (on Ser2) of the RNA pol II C-terminal domain (CTD) (S2P antibody) (Gurtner et al., 2008) (Fig. 6). The topology of active RNA pol II was similar within the nucleus (Fig. 6C,F,I) whatever its position in the pericarp (Fig. 6A), i.e. whatever its ploidy level [according to the ploidy map reported by Bourdon et al. (Bourdon et al., 2011)]. Indeed, active RNA pol II was preferentially associated with less dense chromatin regions as demonstrated by attenuated DAPI staining (e.g. euchromatin; Fig. 6B,E,H) and was excluded from the nuclear periphery where DAPI staining was intense (e.g. heterochromatin; Fig. 6D,G,J).

A nuclear suspension was then prepared from mature green pericarp and immunolabelled with the S2P antibody together with an antibody raised against the unphosphorylated (NP) inactive form of RNA pol II. The fluorescence intensities resulting from each immunolabelling were simultaneously quantified for each ploidy class by cytometry. The S2P and NP immunolabellings were both positively correlated to ploidy levels (Fig. 7A), showing that the protein level for RNA pol II increased proportionally with ploidy. Analysis of double-immunolabelled nuclei confirmed that the

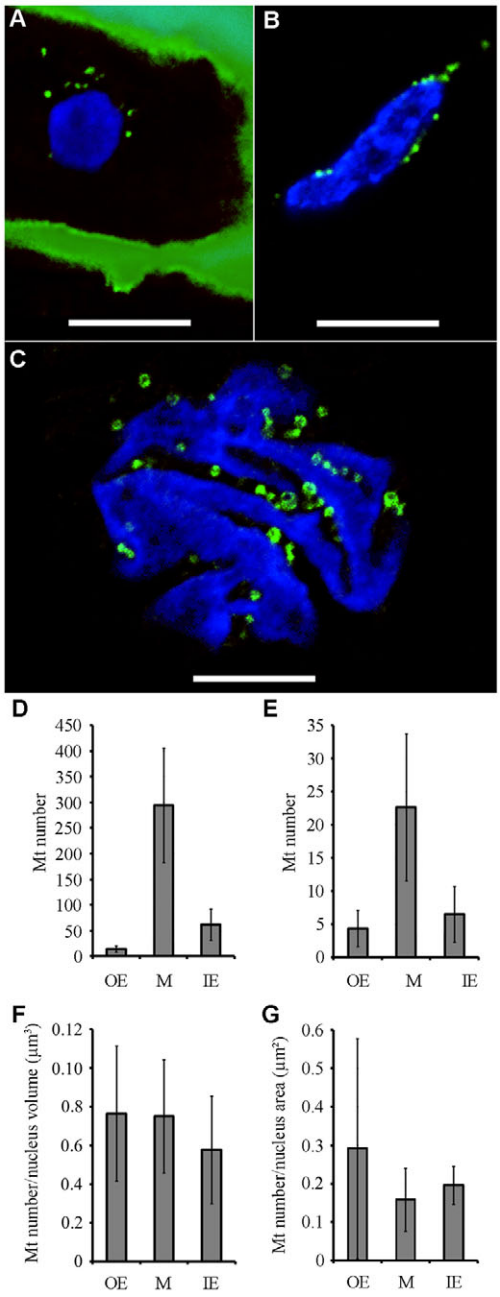

Fig. 4. The population of mitochondria in the vicinity of pericarp nuclei increases with endopolyploidisation. (**A-C**) Single confocal planes of DAPI-stained nuclei (blue) and Rhodamine-123-stained mitochondria (green). The nuclei are in OE (A), IE (B) or M (C). (**D-G**) Enumeration of mitochondria (Mt) on confocal images (D,F) and TEM images (E,G) of nuclei in the three pericarp zones (OE, M and IE). (D) Mean number of mitochondria per nucleus (integration of all the confocal *z*-planes) (Kruskal-Wallis test, $P<10^{-4}$). (E) Mean number of mitochondria per nuclear section (TEM 2D images) (Kruskal-Wallis test, $P<10^{-9}$). (F) Ratio between number of mitochondria and nuclear volume in confocal *z* series. (G) Ratio between number of mitochondria and nuclear area in the TEM section. No significant differences were observed between the pericarp areas (Kruskal-Wallis test, $P>0.08$), whatever the mode of observation (F,G). For confocal images, a total of 52 nuclei (22, 15 and 15 for OE, M and IE, respectively) were analysed and for TEM images 35 single planes of independent nuclei (13, 12 and 10 for OE, M and IE, respectively) were analysed. Error bars indicate s.d. Scale bars: 10 µm.

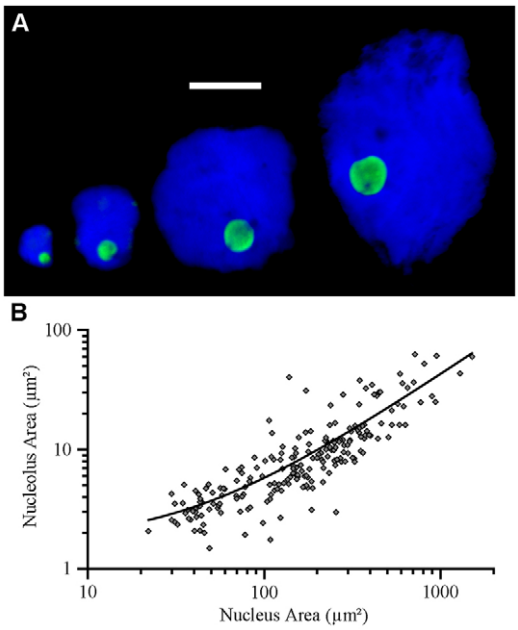

Fig. 5. rRNA transcription increases according to ploidy levels. (**A**) RNA FISH analysis on isolated tomato pericarp nuclei (stained with DAPI, blue) using a 5.8S rRNA probe (green). The images are maximal projections of confocal *z*-series. Scale bar: 10 µm. (**B**) Measurement of the hybridisation signal surface area relative to the nuclear surface area (n=207 nuclei). The equation of the best-fitting curve is y=0.04x+1.65 with R^2=0.67. Note that the axes are on a logarithmic scale.

distribution of S2P immunolabelling appears preferentially associated with euchromatin, as does that of NP (Fig. 7B-E). The labelling of inactive RNA pol II (NP) was highly punctate, possibly at promoter sequences (Fig. 7C), whereas that of the active form (S2P) was homogeneous (Fig. 7D).

The cytometer was used to calculate the immunolabelling intensity ratio (S2P/NP) nucleus by nucleus. For each ploidy class, the coefficients of variation (CV) of this ratio are shown in Fig. 7A. In the 2C and 4C populations, this ratio had a high variance, whereas nuclei of 16C and above were exceptionally uniform, with the ratio having 0.2% CV. The relationship between the phosphorylated and non-phosphorylated states of RNA pol II must be weak in 2C and 4C nuclei, as if multiple nuclear states exist, but it is tight in endoreduplicated nuclei in favour of a uniform nuclear state (for reference, the CV of the DNA peaks typically remain unchanged throughout the ploidy scale).

Endoreduplication correlates with enhanced transcription of endocycle regulating genes

To address gene expression during endoreduplication, we selected five single-copy protein-coding genes in tomato: *RPB1*, which encodes the large subunit of RNA pol II; the endocycle regulating genes *CCS52A* and *WEE1* (Gonzalez et al., 2007; Mathieu-Rivet et al., 2010); and two mitosis-associated genes used as negative controls of gene expression in endoreduplicated nuclei, encoding CDKB2, a cyclin-dependent kinase specific to the G2-M transition (Chevalier, 2007), and the kinetochore MIS12 protein (Sato et al., 2005). qPCR on genomic DNA extracted from 4C, 16C and 32C sorted nuclei confirmed that the extent of all five gene duplications was linearly correlated with the degree of nuclear polyploidisation (supplementary material Fig. S1). Then, real-time qRT-PCR was performed on nuclear RNA extracted from an equal number (~30,000) of 4C, 16C and 32C nuclei to detect the selected five gene transcripts. For each gene, the quantity of transcripts detected in 32C nuclei was used as a reference (relative maximum of expression) for determining transcript levels in 4C and 16C nuclei. As shown in Fig. 8, the amount of *RPB1* transcripts increased according to ploidy levels, in accordance with the observed increase in protein level (Fig. 7A). *CCS52A* and *WEE1* displayed a similar behaviour for transcript accumulation, whereas *CDKB2* and *MIS12* transcripts were undetectable, as expected for mitosis-associated genes. Therefore, despite the correlation between DNA ploidy content and overall transcriptional activity noted above, there is still specificity at the gene transcription level to support physiological functions related to endoreduplication.

DISCUSSION

Recent advances in understanding of the molecular control and function of endoreduplication in higher plants points to its importance in various developmental processes as an essential part of growth (De Veylder et al., 2011). However, little is known about the related cytological aspects, such as the structure of endoreduplicated nuclei and chromosomes or the subcellular modifications associated to endoreduplication in a particular plant tissue and cellular context. As part of our contribution to deciphering the role of endoreduplication during plant development, we aimed here at addressing the influence of ploidy levels on nuclear architecture and on nuclear processes such as transcription.

The polytenic nature of endoreduplicated chromosomes in tomato

As in most angiosperm species (Nagl, 1976; D'Amato, 1984; Joubès and Chevalier, 2000), endoreduplication per se is the main mode of cell endopolyploidisation in tomato fruit tissues (Fig. 1). The use of a highly tandemly repeated DNA sequence probe (2300 copies for 45S rDNA) (Chang et al., 2008) resulted in different hybridisation patterns in FISH assays when compared with non-repeated DNA sequences encoded by bacterial artificial chromosome (BAC) probes, i.e. the presence of two homogeneous large signals for 45S rDNA as compared with two 'clouds' of clustered hybridisation dots for BAC sequences (Bourdon et al., 2011). This difference can be explained by the fact that the 45S rDNA repeats encompass a much larger chromosomal sequence than any BAC probe (respectively, ~20 Mb versus 0.1 Mb on average) (Chang et al., 2008; Bourdon et al., 2011). In addition, untranscribed copies of 45S rDNA are often condensed and located just outside the nucleolus and may contribute to this large hybridisation signal (Heslop-Harrison and Schwarzacher, 2011). The use of a probe specific for the *Arabidopsis* 5S rDNA repeats resulted in hybridisation signals very similar to those for non-repeated DNA sequences (supplementary material Fig. S2) (Bourdon et al., 2011), being organised into two clusters displaying a number of hybridising dots (revealing the chromatids) that correlate with ploidy levels, thus confirming that endopolyploidisation in tomato produces polytenic chromosomes with multivalent sister chromatids. These data support the observation of Schubert et al. (Schubert et al., 2006) of a high degree of sister chromatid separation according to increased endopolyploid levels in *Arabidopsis* nuclei.

The amplification of genomic DNA within endoreduplicated chromosomes is likely to be strictly conservative, as suggested from flow cytometry histograms of pericarp nuclei (Bourdon et al.,

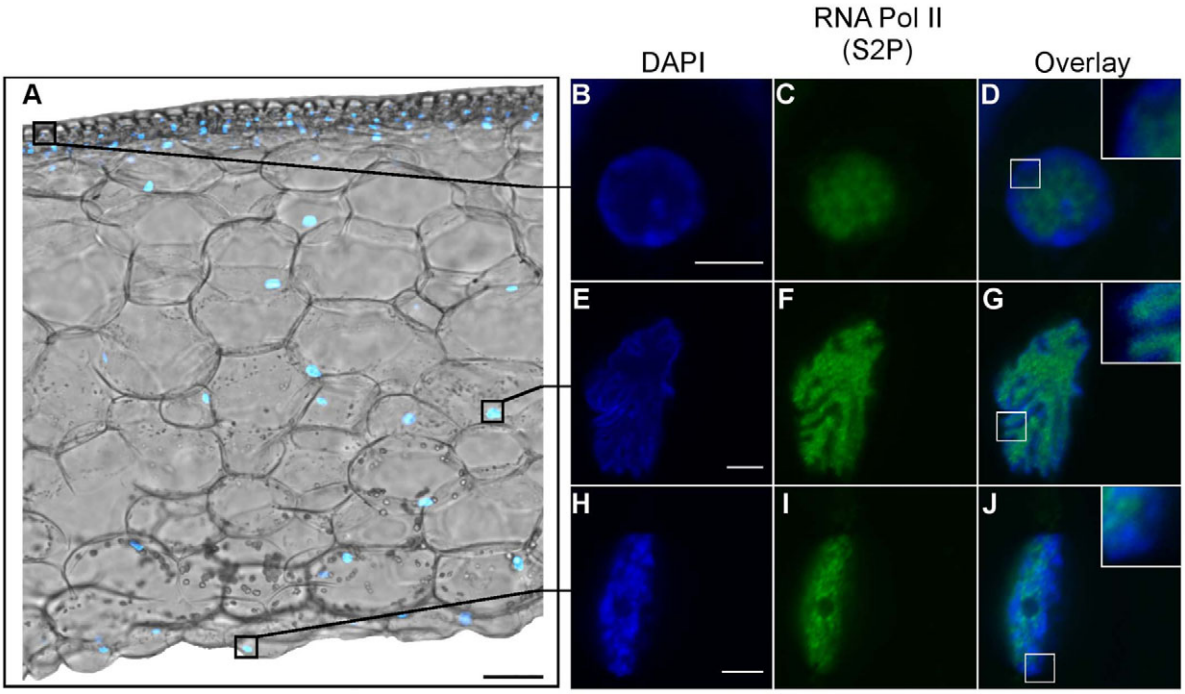

Fig. 6. RNA pol II is homogeneously distributed in euchromatin. (**A**) Location in pericarp of sections shown in B-J. (**B-J**) Immunocytolocalisation of the active form of RNA pol II using S2P antibody as observed in confocal *z*-planes of nuclei in OE (B-D), M (E-G) and IE (H-J). (B,E,H) Chromatin distribution with DAPI. (C,F,I) RNA pol II distribution (Alexa 488). (D,G,J) Overlay of RNA pol II detection (green) and DNA (blue). Insets correspond to a magnification of square regions. Scale bars: 1 mm in A; 5 µm in B-J.

2011). So far, all the single-copy genes or chromosomal regions used as probes in qPCR and FISH experiments, such as 5S rDNA, 45S rDNA, *RPB1*, *CCS52A*, *WEE1*, LE_HBa0048M11 and LE_HBa0037G17 BAC clones (Bourdon et al., 2011), which are respectively located on chromosomes 1, 2, 8, 9, 7 and 12 (Tomato Genome Consortium, 2012; http://solgenomics.net/organism/Solanum_lycopersicum/genome), were found amplified exponentially according to ploidy (Fig. 1; supplementary material Figs S1, S2) (Bourdon et al., 2011). This appears to be a general rule for higher plant endoreduplication, with a notable exception being the developmentally regulated partial endoreduplication observed in orchids (Lepers-Andrzejewski et al., 2011).

Endoreduplication leads to larger nuclei with conserved karyoplasmic exchange ability

Our previous analysis of the ploidy distribution across tomato fruit pericarp showed no evidence for any positive correlation between endoreduplication and cell fate, as a definite ploidy level cannot be assigned to a precise cell size or cell fate (Bourdon et al., 2011). Although the positive correlation between endoreduplication and cell size has been described in wild-type tomato fruits (Cheniclet et al., 2005; Nafati et al., 2011), we have shown that there is a broad variety of cell types from IE to OE according to a complex differentiation pattern during fruit development, including a large discrepancy in cell sizes with partially overlapping ploidy levels (Bourdon et al., 2011). These data and additional functional studies led us to propose that endoreduplication serves as a trigger for organ growth and provides the potential to support a range of cell sizes rather than any precise, definitive size (Mathieu-Rivet et al., 2010; Nafati et al., 2011).

The nuclear morphology of endoreduplicated cells in tomato pericarp is strongly affected by endopolyploidisation, with highly invaginated and grooved nuclear envelopes (Fig. 2). Such characteristics have already been reported for plant and animal nuclei (Fricker et al., 1997; Collings et al., 2000). Interestingly, the endoreduplicated and invaginated nuclei can maintain their exchange ability during endopolyploidisation (Fig. 3B). The exchange ability is related to the distance to be travelled by molecules from their site of synthesis within the nucleus to their export site on the envelope. For a circle the maximum distance between any point within the circle and the periphery is equal to its radius. The fact that nuclei larger than 20 µm in radius display an exchange ability (estimated by the P/A ratio) similar to that of nuclei (or circles) of 3.3 µm radius suggests that their complex shape minimises the distance between the inner volume and the envelope of the nucleus. In addition, the pronounced invaginations of endoreduplicated nuclei enable the maintenance of efficient nucleus-to-cytoplasm communication, despite the increase in nuclear volume. Indeed, numerous mitochondria were found to be localised in the grooves of the nuclear envelope (Fig. 4), i.e. at the site of cytoplasm-to-nucleus exchange. Such a direct proportionality between nuclear DNA content and the number of organelles – at least for plastids – has been reported (D'Amato, 1998). In addition, labelling with JC-1 dye to examine mitochondrial membrane potential revealed that mitochondria were largely active whatever the pericarp area considered (supplementary material Fig. S3). Therefore, the presence of a large population of functional mitochondria close to the envelope of endoreduplicated nuclei could be explained by an absolute need for ATP synthesis as an energy supply for nuclear biochemical processes. Thus, our observation at the cellular level supports the commonly inferred, but not experimentally demonstrated, association of endopolyploidy with metabolically highly active cells (Larkins et al., 2001; Sugimoto-Shirasu and Roberts, 2003).

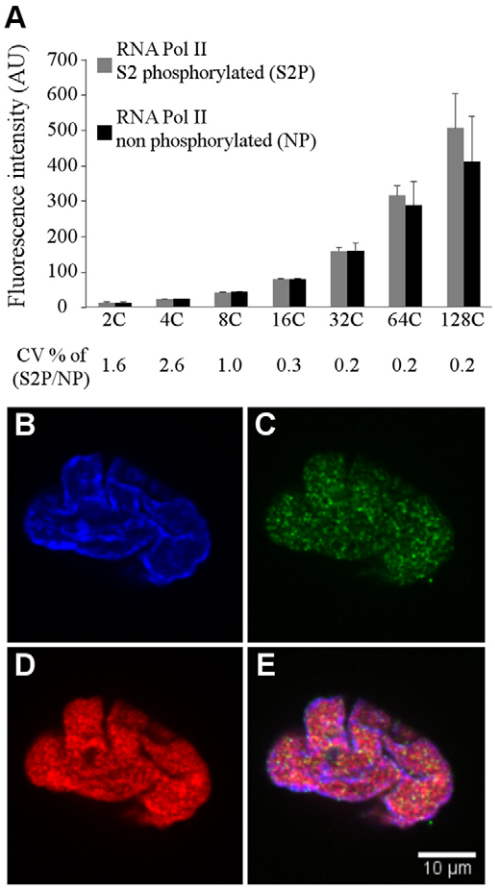

Fig. 7. The amount of RNA pol II increases according to ploidy levels. (**A**) Fluorescence intensity from cytometry of double-immunolabelled nuclei using the S2P and NP RNA pol II antibodies. For each ploidy class, the coefficient of variation (CV%) of the parameter 'S2P/NP ratio of each nucleus' is indicated (see text for interpretation). Error bars indicate s.d. (**B-E**) Phosphorylated and non-phosphorylated RNA pol II in confocal *z*-plane of an isolated nucleus. (B) Chromatin DNA revealed by DAPI. (C) Distribution of NP RNA pol II (Alexa 488). (D) Distribution of S2P RNA pol II (Alexa 633). (E) Overlay of B-D. Scale bar: 10 µm.

Endoreduplication triggers enhanced transcriptional activity

The highly polyploid endosperm cells of maize kernels, which accumulate large amounts of starch and storage proteins (Sabelli and Larkins, 2009), and the nitrogen-fixing symbiotic root nodule cells in legumes (Cebolla et al., 1999) are quoted as metabolically specialised and highly endoreduplicated cells. Interestingly, an important remodelling of the transcriptome is tightly linked to endoreduplication in nitrogen-fixing nodules (Mergaert et al., 2003). As far as tomato fruit is concerned, only descriptive analyses for transcriptional and metabolic profiling in endoreduplicated tissues have been provided (Lemaire-Chamley et al., 2005; Mounet et al., 2009; Schauer et al., 2006; Steinhauser et al., 2010), without any direct link with the extent of endoreduplication.

Using RNA FISH we demonstrated that the transcription of 5.8S rDNA within the nucleolus is enhanced during endoreduplication (Fig. 5). In addition, the 5.8S rRNA hybridisation signal that reflects the size of the nucleolus was positively correlated with nuclear size and consequently with ploidy levels. These data are

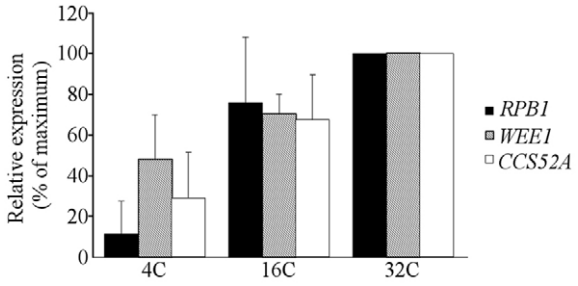

Fig. 8. Transcript levels of *RPB1*, *WEE1* and *CCS52A* increase according to ploidy levels. The expression of *RPB1*, *WEE1* and *CCS52A* in nuclei sorted at different ploidy levels (4C, 16C and 32C) was assessed by qRT-PCR. Data are the mean of three biological replicates. Error bars indicate s.d.

consistent with our observation of NOR enlargement according to ploidy (Fig. 1B). Such a nucleolar enlargement has been reported in rodent trophoblasts (Zybina and Zybina, 1996) and in *Drosophila* (Pierce et al., 2004) and associated with increased transcriptional and translational activities in the context of endopolyploidisation. This feature has also been associated with the rate of proliferation in cancer cells (Derenzini et al., 2000). It is therefore tempting to draw a parallel with the increased rate of growth that is often associated with endoreduplication. We found that the cytoplasmic area of cells within the three most contrasting pericarp zones in terms of ploidy levels (OE, IE and M, where the most common nuclear classes are 2C, 16C and 64C, respectively) indeed increases with ploidy levels (supplementary material Fig. S4A), as does the estimated cytoplasmic volume (supplementary material Fig. S4B). This demonstrates the maintenance of the nuclear to cytoplasmic ratio to drive cell growth, consistent with the karyoplasmic ratio theory. Ribosomal RNA, protein synthesis and exchange must be proportionally enhanced to increase ribosome biogenesis and hence maintain homeostasis of cytoplasmic components essential for sustained cell growth.

Previous functional analyses of genes regulating the endocycle (Gonzalez et al., 2007; Mathieu-Rivet et al., 2010; Nafati et al., 2011) demonstrated the biological significance of endoreduplication as a morphogenetic factor for cell and fruit growth in tomato. In addition, enhancing endoreduplication and consequently fruit growth also strongly impacted nitrogen metabolism in developing fruits (Mathieu-Rivet et al., 2010), establishing a link between endoreduplication-induced growth and primary metabolism, as reported in maize endosperm (Leiva-Neto et al., 2004). Interestingly, a causal relationship between cell size, polyploidy and transcription in yeast has been demonstrated, suggesting that cells adjust their transcriptional capacities to their geometric properties, including cell size (Wu et al., 2010).

Here, we showed that transcription of the *WEE1* and *CCS52A* genes that control endoreduplication (Gonzalez et al., 2007; Mathieu-Rivet et al., 2010) is increased on a per-nucleus basis according to ploidy (Fig. 8). This observation was also true for *RPB1*, which encodes a subunit of RNA pol II. The use of polyclonal antibodies targeting the YSPTSPS repeat of the RNA pol II CTD allowed us to discriminate between the active and inactive status of RNA pol II. The RNA pol II CTD repeat is differentially phosphorylated according to its position on a gene: when located on a promoter sequence, it is largely unphosphorylated (NP form), whereas the active form of RNA pol II requires phosphorylation at Ser2 and Ser5 (Hirose and Ohkuma,

2007). In addition, phosphorylation at Ser5 is mainly associated with the initiation of transcription (Hengartner et al., 1998; Komarnitsky et al., 2000), whereas phosphorylation at Ser2 (S2P form) is predominantly present during the elongation step of transcription (Ni et al., 2004). Endoreduplication is linked to the sustained transcription/translation and activity of *RPB1* (Figs 6, 7). Furthermore, the results obtained with the S2P antibody suggest that transcriptional elongation is excluded from the perinuclear heterochromatic region and occurs within euchromatin in a homogeneous manner (Fig. 6). Subnuclear compartments were not evident, suggesting that the euchromatin regions in polyploid nuclei are apparently indiscriminately transcribed, as if all copies of amplified genes are equally functional in the tomato endoreduplicated genome. Moreover, the exceptionally tight CV observed for the S2P/NP ratio in polyploid nuclei (Fig. 7) reveals a uniformity of transcriptional activity when compared with that observed in 2C and 4C nuclei. Altogether, these results demonstrate a strong relationship between endoreduplication and transcription.

Conclusions

The role of endoreduplication in organ growth is still a matter of debate. An organismal regulation of growth in which organ growth itself acts as a 'hub' driving cell division and expansion, as well as endoreduplication, with compensation if one of the underlying cellular processes is limiting (John and Qi, 2008; Massonnet et al., 2011), is opposed to a cell-based (autonomous) mode of growth control that relies on the balance of cellular processes (division, expansion and endoreduplication) (Sugimoto-Shirasu and Roberts, 2003).

The results presented here provide quantitative evidence in favour of the karyoplasmic ratio theory. Different levels of specific structural and functional organisation in endoreduplicated cells were revealed, shedding light on the contribution of endoreduplication to the establishment of a highly structured cellular system that integrates multiple physiological functions, including transcription, and acts as a morphogenetic factor supporting cell growth during tomato fruit development. Our perspective is that karyoplasmic homeostasis ensures function not only by geometry, but also by cooperative adaptation.

Acknowledgements

Image acquisition and analysis were performed at the Plant Imaging Pole of the Bordeaux Imaging Center. Flow cytometry was performed at the Imagif Platform (IFR87 and ASTRE, CNRS, Gif-sur-Yvette) with Marie-Noëlle Soler, whom we thank for help with imaging. We thank Norbert Bollier for contribution to the results obtained on mitochondria.

Funding

This work was carried out with the financial support of the French Agence Nationale de la Recherche [grant ANR-09-GENM-105].

Competing interests statement

The authors declare no competing financial interests.

Supplementary material

Supplementary material available online at
http://dev.biologists.org/lookup/suppl/doi:10.1242/dev.084053/-/DC1

References

Adachi, S., Minamisawa, K., Okushima, Y., Inagaki, S., Yoshiyama, K., Kondou, Y., Kaminuma, E., Kawashima, M., Toyoda, T., Matsui et al. (2011). Programmed induction of endoreduplication by DNA double-strand breaks in Arabidopsis. *Proc. Natl. Acad. Sci. USA* **108**, 10004-10009.

Arumuganathan, K., Martin, G. B., Telenius, H., Tanksley, S. D. and Earle, E. D. (1994). Chromosome 2-specific DNA clones from flow-sorted chromosomes of tomato. *Mol. Gen. Genet.* **242**, 551-558.

Barow, M. (2006). Endopolyploidy in seed plants. *BioEssays* **28**, 271-281.

Bourdon, M., Coriton, O., Cheniclet, C., Brown, S., Poujol, C., Chevalier, C., Renaudin, J.-P., Frangne, N. (2011). In planta quantification of endopolyploidy using fluorescent in situ hybridization (FISH). *Plant J.* **66**, 1089-1099.

Bramsiepe, J., Wester, K., Weinl, C., Roodbarkelari, F., Kasili, R., Larkin, J. C., Hülskamp, M. and Schnittger, A. (2010). Endoreplication controls cell fate maintenance. *PLoS Genet*. **6**, e1000996.

Brodsky, W. Y. and Uryvaeva, I. V. (1977). Cell polyploidy: its relation to tissue growth and function. *Int. Rev. Cytol.* **50**, 275-332.

Carde, J. P. (1987). Electron microscopy of plant cell membranes. *Methods Enzymol*. **148**, 599-622.

Cebolla, A., Maria Vinardell, J., Kiss, E., Olah, B., Roudier, F., Kondorosi, A. and Kondorosi, E. (1999). The mitotic inhibitor ccs52 is required for endoreduplication and ploidy-dependent cell enlargement in plants. *EMBO J*. **18**, 4476-4484.

Ceccarelli, M., Sanantonio, E., Marmottini, F., Amzallag, G. N. and Cionini, P. G. (2006). Chromosome endoreduplication as a factor of salt adaptation in *Sorghum bicolor. Protoplasma* **227**, 113-118.

Chang, S.-B., Yang, T.-J., Datema, E., van Vugt, J., Vosman, B., Kuipers, A., Meznikova, M., Szinay, D., Lankhorst, R., Jacobsen, E. and de Jong, H. (2008). FISH mapping and molecular organization of the major repetitive sequences of tomato. *Chromosome Res.* **16**, 919-933.

Cheniclet, C., Rong, W. Y., Causse, M., Frangne, N., Bolling, L., Carde, J.-P. and Renaudin, J.-P. (2005). Cell expansion and endoreduplication show a large genetic variability in pericarp and contribute strongly to tomato fruit growth. *Plant Physiol.* **139**, 1984-1994.

Chevalier, C. (2007). Cell cycle control and fruit development. In *Annual Plant Reviews Volume 32: Cell Cycle Control and Plant Development* (ed. D. Inzé), pp. 269-293. Oxford, UK: Blackwell Publishing.

Chevalier, C., Nafati, M., Mathieu-Rivet, E., Bourdon, M., Frangne, N., Cheniclet, C., Renaudin, J.-P., Gévaudant, F., Hernould, M. (2011). Elucidating the functional role of endoreduplication in tomato fruit development. *Ann. Bot.* **107**, 1159-1169.

Collings, D. A., Carter, C. N., Rink, J. C., Scott, A. C., Wyatt, S. E. and Allen, N. S. (2000). Plant nuclei can contain extensive grooves and invaginations. *Plant Cell* **12**, 2425-2440.

Cookson, S. J., Radziejwoski, A. and Granier, C. (2006). Cell and leaf size plasticity in *Arabidopsis*: what is the role of endoreduplication? *Plant Cell Environ.* **29**, 1273-1283.

D'Amato, F. (1984). Role of polyploidy in reproductive organs and tissues. In *Embryology of Angiosperms* (ed. B. M. Johri), pp. 519-566. New York: Springer.

D'Amato, F. (1998). Chromosome endoreduplication in plant tissue development and function. In *Plant Cell Proliferation and its Regulation in Growth and Development* (ed. J. A. Bryant and D. Chiatante), pp. 153-166. Chichester: J. Wiley & Sons.

De Veylder, L., Larkin, J. C. and Schnittger, A. (2011). Molecular control and function of endoreduplication in development and physiology. *Trends Plant Sci.* **16**, 624-634.

Derenzini, M., Trere, D., Pession, A., Govoni, M., Sirri, V. and Chieco, P. (2000). Nucleolar size indicates the rapidity of cell proliferation in cancer tissues. *J. Pathol.* **191**, 181-186.

Emaus, R. K., Grunwald, R. and Lemasters, J. J. (1986). Rhodamine-123 as a probe of transmembrane potential in isolated rat-liver mitochondria – spectral and metabolic properties. *Biochem. Biophys. Acta* **850**, 436-448.

Fricker, M., Hollinshead, M., White, N. and Vaux, D. (1997). Interphase nuclei of many mammalian cell types contain deep, dynamic, tubular membrane-bound invaginations of the nuclear envelope. *J. Cell Biol.* **136**, 531-544.

Galbraith, D. W., Janda, J. and Lambert, G. M. (2011). Multiparametric analysis, sorting, and transcriptional profiling of plant protoplasts and nuclei according to cell type. *Methods Mol. Biol.* **699**, 407-429.

Gerlach, W. L. and Bedbrook, J. R. (1979). Cloning and characterization of ribosomal RNA genes from wheat and barley. *Nucleic Acids Res.* **7**, 1869-1885.

Gonzalez, N., Gevaudant, F., Hernould, M., Chevalier, C. and Mouras, A. (2007). The cell cycle-associated protein kinase WEE1 regulates cell size in relation to endoreduplication in developing tomato fruit. *Plant J.* **51**, 642-655.

Gurtner, A., Fuschi, P., Magi, F., Colussi, C., Gaetano, C., Dobbelstein, M., Sacchi, A. and Piaggio, G. (2008). NF-Y dependent epigenetic modifications discriminate between proliferating and postmitotic tissue. *PLoS ONE* **3**, e2047.

Hase, Y., Trung, K. H., Matsunaga, T. and Tanaka, A. (2006). A mutation in the uvi4 gene promotes progression of endo-reduplication and confers increased tolerance towards ultraviolet B light. *Plant J.* **46**, 317-326.

Hengartner, C. J., Myer, V. E., Liao, S. M., Wilson, C. J., Koh, S. S. and Young, R. A. (1998). Temporal regulation of RNA polymerase II by Srb10 and Kin28 cyclin-dependent kinases. *Mol. Cell* **2**, 43-53.

Hernandez-Verdun, D. (2006). Nucleolus: from structure to dynamics. *Histochem. Cell Biol.* **125**, 127-137.

Heslop-Harrison, J. S. and Schwarzacker, T. (2011). Organization of the plant genome in chromosomes. *Plant J*. **66**, 18-33.

Hirose, Y. and Ohkuma, Y. (2007). Phosphorylation of the C-terminal domain of RNA polymerase II plays central roles in the integrated events of eucaryotic gene expression. *J. Biochem.* **141**, 601-608.

Hülskamp, M., Schnittger, A. and Folkers, U. (1999). Pattern formation and cell differentiation: trichomes in Arabidopsis as a genetic model system. *Int. Rev. Cytol.* **186**, 147-178.
Ishida, T., Kurata, T., Okada, K. and Wada, T. (2008). A genetic regulatory network in the development of trichomes and root hairs. *Ann. Rev. Plant Biol.* **59**, 365-386.
Jo, S.-H., Koo, D.-H., Kim, J., Hur, C.-G., Lee, S., Yang, T.-j., Kwon, S.-Y. and Choi, D. (2009). Evolution of ribosomal DNA-derived satellite repeat in tomato genome. *BMC Plant Biol.* **9**, 42.
John, P. C. L. and Qi, R. (2008). Cell division and endoreduplication: doubtful engines of vegetative growth. *Trends Plant Sci.* **13**, 121-127.
Jolly, C., Mongelard, F., Robert-Nicoud, M. and Vourc'h, C. (1997). Optimization of nuclear transcript detection by FISH and combination with fluorescence immunocytochemical detection of transcription factors. *J. Histochem. Cytochem.* **45**, 1585-1592.
Joubès, J. and Chevalier, C. (2000). Endoreduplication in higher plants. *Plant Mol. Biol.* **43**, 735-745.
Komarnitsky, P., Cho, E. J. and Buratowski, S. (2000). Different phosphorylated forms of RNA polymerase II and associated mRNA processing factors during transcription. *Genes Dev.* **14**, 2452-2460.
Larkins, B. A., Dilkes, B. P., Dante, R. A., Coelho, C. M., Woo, Y.-m. and Liu, Y. (2001). Investigating the hows and whys of DNA endoreduplication. *J. Exp. Bot.* **52**, 183-192.
Lee, H. O., Davidson, J. M. and Duronio, R. J. (2010). Endoreduplication: polyploidy with purpose. *Genes Dev*. **23**, 2461-2477.
Leiva-Neto, J. T., Grafi, G., Sabelli, P. A., Dante, R. A., Woo, Y. M., Maddock, S., Gordon-Kamm, W. J. and Larkins, B. A. (2004). A dominant negative mutant of cyclin-dependent kinase A reduces endoreduplication but not cell size or gene expression in maize endosperm. *Plant Cell* **16**, 1854-1869.
Lemaire-Chamley, M., Petit, J., Garcia, V., Just, D., Baldet, P., Germain, V., Fagard, M., Mouassite, M., Cheniclet, C. and Rothan, C. (2005). Changes in transcriptional profiles are associated with early fruit tissue specialization in tomato. *Plant Physiol.* **139**, 750-769.
Lepers-Andrzejewski, S., Siljak-Yakovlev, S., Brown, S. C., Wong. M. and Dron, M. (2011). Diversity and dynamics of plant genome size: an example of polysomaty from a cytogenetic study of Tahitian Vanilla (*Vanilla xtahitensis*, Orchidaceae). *Am. J. Bot.* **98**, 986-997.
Massonnet, C., Tisné, S., Radziejwoski, A., Vile, D., De Veylder, L., Dauzat, M. and Granier, C. (2011). New insights into the control of endoreduplication: endoreduplication could be driven by organ growth in *Arabidopsis* leaves. *Plant Physiol.* **157**, 2044-2055.
Mathieu-Rivet, E., Gevaudant, F., Sicard, A., Salar, S., Do, P. T., Mouras, A., Fernie, A. R., Gibon, Y., Rothan, C., Chevalier, C. and Hernould, M. (2010). Functional analysis of the anaphase promoting complex activator CCS52A highlights the crucial role of endo-reduplication for fruit growth in tomato. *Plant J.* **62**, 727-741.
Mergaert, P., Nikovics, K., Kelemen, Z., Maunoury, N., Vaubert, D., Kondorosi, A. and Kondorosi, E. (2003). A novel family in *Medicago truncatula* consisting of more than 300 nodule-specific genes coding for small, secreted polypeptides with conserved cysteine motifs. *Plant Physiol.* **132**, 161-173.
Mounet, F., Moing, A., Garcia, V., Petit, J., Maucourt, M., Deborde, C., Bernillon, S., Le Gall, G., Colquhoun, I., Defernez, M. et al. (2009). Gene and metabolite regulatory network analysis of early developing fruit tissues highlights new candidate genes for the control of tomato fruit composition and development. *Plant Physiol.* **149**, 1505-1528.
Nafati, M., Cheniclet, C., Hernould, M., Do, P. T., Fernie, A., Chevalier, C., Gévaudant, F. (2011). The specific overexpression of a cyclin dependent kinase inhibitor in tomato fruit mesocarp cells uncouples endoreduplication and cell growth. *Plant J.* **65**, 543-556.
Nagl, W. (1976). DNA endoreduplication and polyteny understood as evolutionary strategies. *Nature* **261**, 614-615.
Ni, Z., Schwartz, B. E., Werner, J., Suarez, J. R. and Lis, J. T. (2004). Coordination of transcription, RNA processing, and surveillance by P-TEFb kinase on heat shock genes. *Mol. Cell* **13**, 55-65.
Pierce, S. B., Yost, C., Britton, J. S., Loo, L. W. M., Flynn, E. M., Edgar, B. A. and Eisenman, R. N. (2004). dMyc is required for larval growth and endoreplication in *Drosophila*. *Development*, **131**, 2317-2327.
Roeder, A. H. K., Chickarmane, V., Cunha, A., Obara, B., Manjunath, B. S. and Meyerowitz, E. M. (2010). Variability in the control of cell division underlies sepal epidermal patterning in *Arabidopsis thaliana*. *PLoS Biol*. **8**, e1000367.
Rudra, D. and Warner, J. R. (2004). What better measure than ribosome synthesis? *Genes Dev.* **18**, 2431-2436.
Sabelli, P. A. and Larkins, B. A. (2009). The contribution of cell cycle regulation to endosperm development. *Sex. Plant Reprod.* **22**, 207-219.
Sato, H., Shibata and F., Murata, M. (2005). Characterization of a MIS12 homologue in *Arabidopsis thaliana*. *Chromosome Res.* **13**, 827-834.
Schauer, N., Semel, Y., Roessner, U., Gur, A., Balbo, I., Carrari, F., Pleban, T., Perez-Melis, A., Bruedigam, C., Kopka, J. et al. (2006). Comprehensive metabolic profiling and phenotyping of interspecific introgression lines for tomato improvement. *Nat. Biotech.* **24**, 447-454.
Schubert, V., Klatte, M., Pecinka, A., Meister, A., Jasencakova, Z. and Schubert, I. (2006). Sister chromatids are often incompletely aligned in meristematic and endopolyploid interphase nuclei of *Arabidopsis thaliana*. *Genetics* **172**, 467-475.
Steinhauser, M. C., Steinhauser, D., Koehl, K., Carrari, F., Gibon, Y., Fernie, A. R. and Stitt, M. (2010). Enzyme activity profiles during fruit development in tomato cultivars and *Solanum pennellii*. *Plant Physiol.* **153**, 80-98.
Sugimoto-Shirasu, K. and Roberts, K. (2003). 'Big it up': endoreduplication and cell-size control in plants. *Curr. Opin. Plant Biol.* **6**, 544-553.
Terasaki, M. and Reese, T. S. (1992). Characterization of endoplasmic reticulum by co-localization of BiP and dicarbocyanine dyes. *J. Cell Sci.* **101**, 315-322.
Tomato Genome Consortium (2012). The tomato genome sequence provides insights into fleshy fruit evolution. *Nature* **485**, 635-641.
Wu, C.-Y., Rolfe, P. A., Gifford, D. K. and Fink, G. R. (2010). Control of transcription by cell size. *PLoS Biol.* **8**, e1000523.
Zybina, E. V. and Zybina, T. G. (1996). Polytene chromosomes in mammalian cells. *Int. Rev. Cytol.* **165**, 53-119.

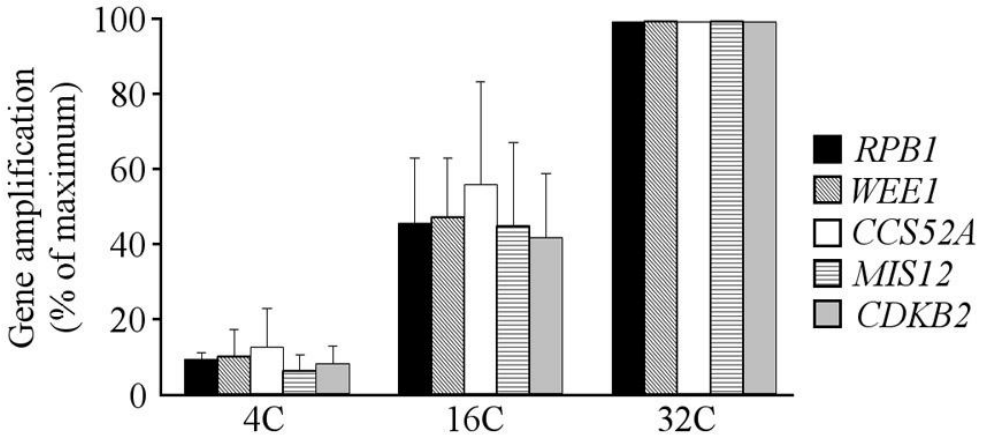

Fig. S1. Quantification of *RPB1*, *WEE1*, *CCS52A*, *MIS12* and *CDKB2* gene amplification according to ploidy levels. The gene amplification of *RPB1*, *WEE1*, *CCS52A*, *MIS12* and *CDKB2* was assessed by qPCR using 100 nuclei sorted at different ploidy levels (4C, 16C and 32C). Data are the mean of three biological repetitions.

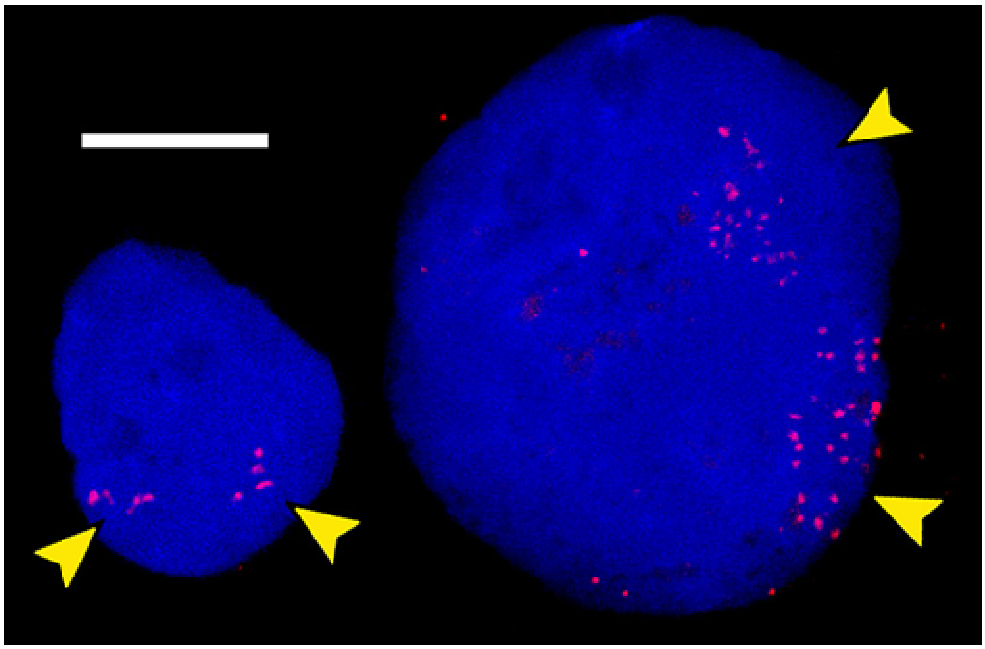

Fig. S2. DNA FISH on isolated nuclei using the *Arabidopsis* 5S rDNA probe. Two pericarp nuclei of different size are represented. Images are maximal projections of confocal *z*-series. The hybridisation signal is clustered in two groups of red dots (yellow arrows) and the difference in dot number indicates contrasting ploidy levels for the two nuclei. Chromatin is stained with DAPI (blue). Scale bar: 10 µm.

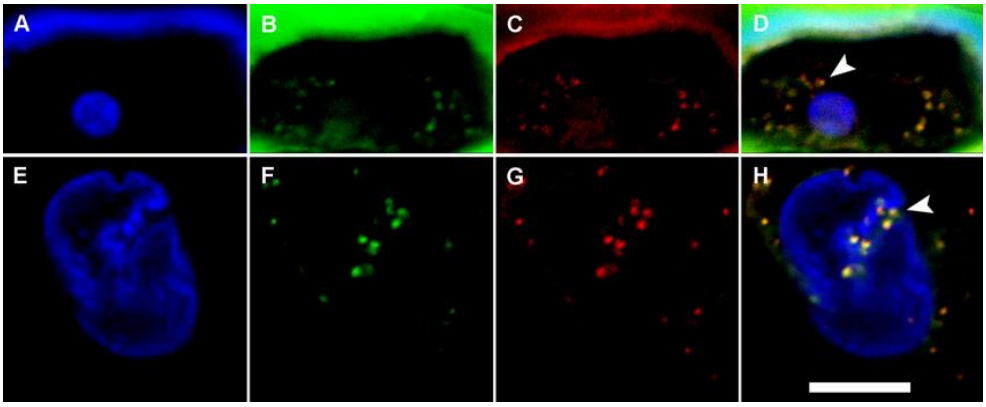

Fig. S3. Viability analysis of mitochondria surrounding endoreduplicated nuclei. (**A-H**) Confocal images (single planes) of DAPI-stained nuclei (blue) and JC-1-stained mitochondria from pericarp areas displaying contrasting ploidy levels: (A-D) outer epidermis (2C-4C levels) and (E-H) mid-mesocarp (32C-128C levels). (A,E) DAPI staining; (B,F) detection of JC-1 monomers (green, 520 nm); (C,G) detection of JC-1 aggregates (red, 585 nm), revealing the maintenance of membrane mitochondrial potential; (D,H) overlay. Pericarp pieces were stained for 7 minutes at room temperature in the presence of DAPI (5 µg/ml) and JC-1 (3.8 µM) in PBS, then briefly washed in PBS and observed under a confocal microscope. The excitation (Ex) and emission (Em) wavelengths were: for detection of JC-1 monomers, Ex 488 nm and Em 515-540 nm; for detection of JC-1 aggregates, Ex 543 nm and Em 580-615 nm. Arrowheads in D,H point to mitochondria. Scale bar: 10 µm.

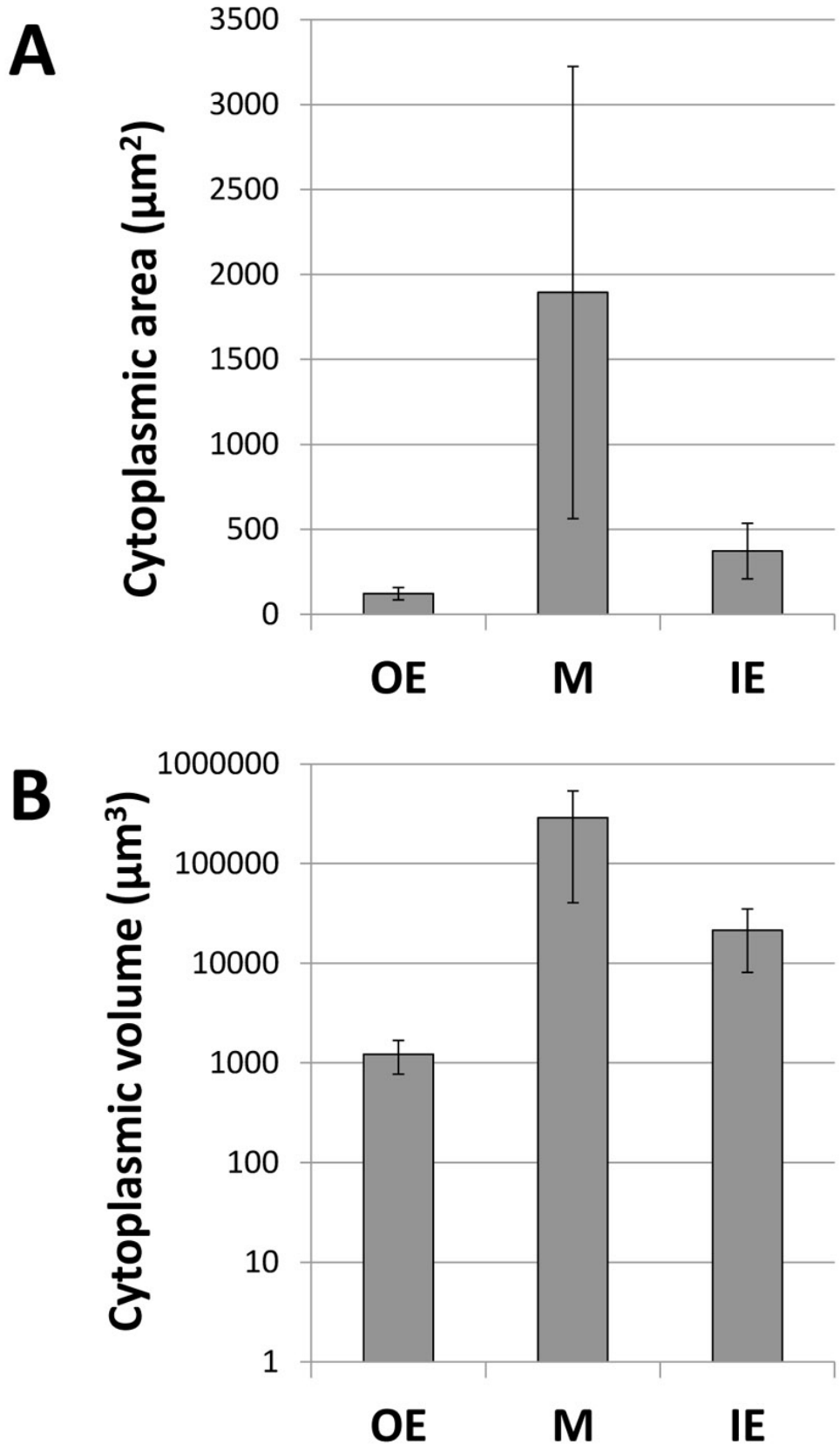

Fig. S4. Cytoplasmic area and volume are adjusted relative to cell position within the three most contrasting pericarp zones in terms of ploidy level. (**A**) Cytoplasmic area according to cell position across pericarp (OE, M and IE) was assessed on photon microscopy images of 1 µm Epon-embedded fruit pericarp sections stained with Toluidine Blue, by excluding the nuclear and vacuolar compartments, using Image-Pro Plus software. The most common nuclear classes in these tissues are, respectively, 2C, 64C and 16C (Bourdon et al., 2011). (**B**) Cytoplasmic volume was estimated from measurements of cytoplasmic area, cell perimeter and cell diameter from (A) as follows. First, cell volume (V_1) was calculated from

maximal (a) and minimal (b) radii measured on sections, assuming that cells have the shape of a revolution ellipsoid [$V_1=(4/3)*\pi*a*b^2$]. Second, mean cytoplasmic thickness (t) was estimated by dividing cytoplasmic area by cell perimeter; this approximation can be made because the cytoplasm only represents a very thin layer close to the cell periphery. Third, we calculated the óvacuolarô volume (V_2) of an ellipsoid with maximal and minimal radii of (a-t) and (b-t), respectively. Finally, the cytoplasmic volume was deduced as the difference: V_1ï V_2. Note that a logarithmic scale is used for the *y*-axis. OE, outer epidermis (*n*=18); M, mesocarp (*n*=23); IE, inner epidermis (*n*=15).

Table S1. PCR primers used for the synthesis of tomato 5.8S RNA probes for RNA FISH

Gene	Primer sequence (5′-3′)
Antisense probe	
Forward	TAATACGACTCACTATAGGGACAAACGACTCTCGGCAAC
Reverse	CGTGACGCCCAGGCAGACGTGCCCTCGGCCAAATGGCTTC
Sense probe (negative control)	
Forward	ACAAACGACTCTCGGCAACGGATATCTCGGCTCTCGCAT
Reverse	TAATACGACTCACTATAGGGAGGCAGACGTGCCCTCG

The sequence of the T7 promoter used for T7 RNA polymerase transcription is underlined.

Table S2. Primers used in qPCR to amplify genomic DNA or cDNA and size of amplified products

Gene	Primer sequence (5′-3′)	Expected size (bp)	SGN gene ID / accession number
Solly;*WEE1*			
Sense	CAAATTTGAAATCTCCCCAA	104	Solyc09g074830 /
Antisense	TGGAAATGGATCTTCTTGTA		AM180939
Solly;*CCS52A*			
Sense	AAACCCCATCAAGAACAAAT	102	Solyc08g080080 /
Antisense	AAGATCTACTCGGAATGAAA		FN556057
Solly;*RPB1*	(For genomic amplification)		
Sense	ATAGCGTAAGTTAGCGACCTGAT	105	Solyc02g083350
Antisense	TCAGAAAGGAGGCTTTAAGAA		
Solly;*RPB1*	(For cDNA amplification)		
Sense	CTGTGGTGCACATTGAGCAT	105	SGN-U586520
Antisense	CACACTTCATCTTCCGATCAAT		
Solly;*CDKB2*;1			
Sense	CACAAACACAGCGAGAGTGAA	95	Solyc04g082840 /
Antisense	CCAACCTTCTCCAGCTTCTC		AJ297917
Solly;*MIS12*			
Sense	GGTGTTCGATTCATTGAACCTA	92	Solyc03g114520 /
Antisense	AGAAATCGAAAGCATCGTCA		SGN-U563789